Supporting information

Immobilized graphene nanoflakes micro-pattern device for high-throughput uniform intracellular biomolecular delivery

Donia Dominic[a], Rajdeep Ojha[b], Moeto Nagai[c], Srabani Kar[a, d], Tuhin Subhra Santra[a]*

[a]Department of Engineering Design, Indian Institute of Technology Madras, India
[b]Department of Physical Medicine and Rehabilitation, Christian Medical College, India
[c]Department of Mechanical Engineering, Toyohashi University of Technology, Japan
[d]Department of Physics, Indian Institute of Technology, Hyderabad, India

Corresponding author: Tuhin Subhra Santra, tuhin@smail.iitm.ac.in, santra.tuhin@gmail.com

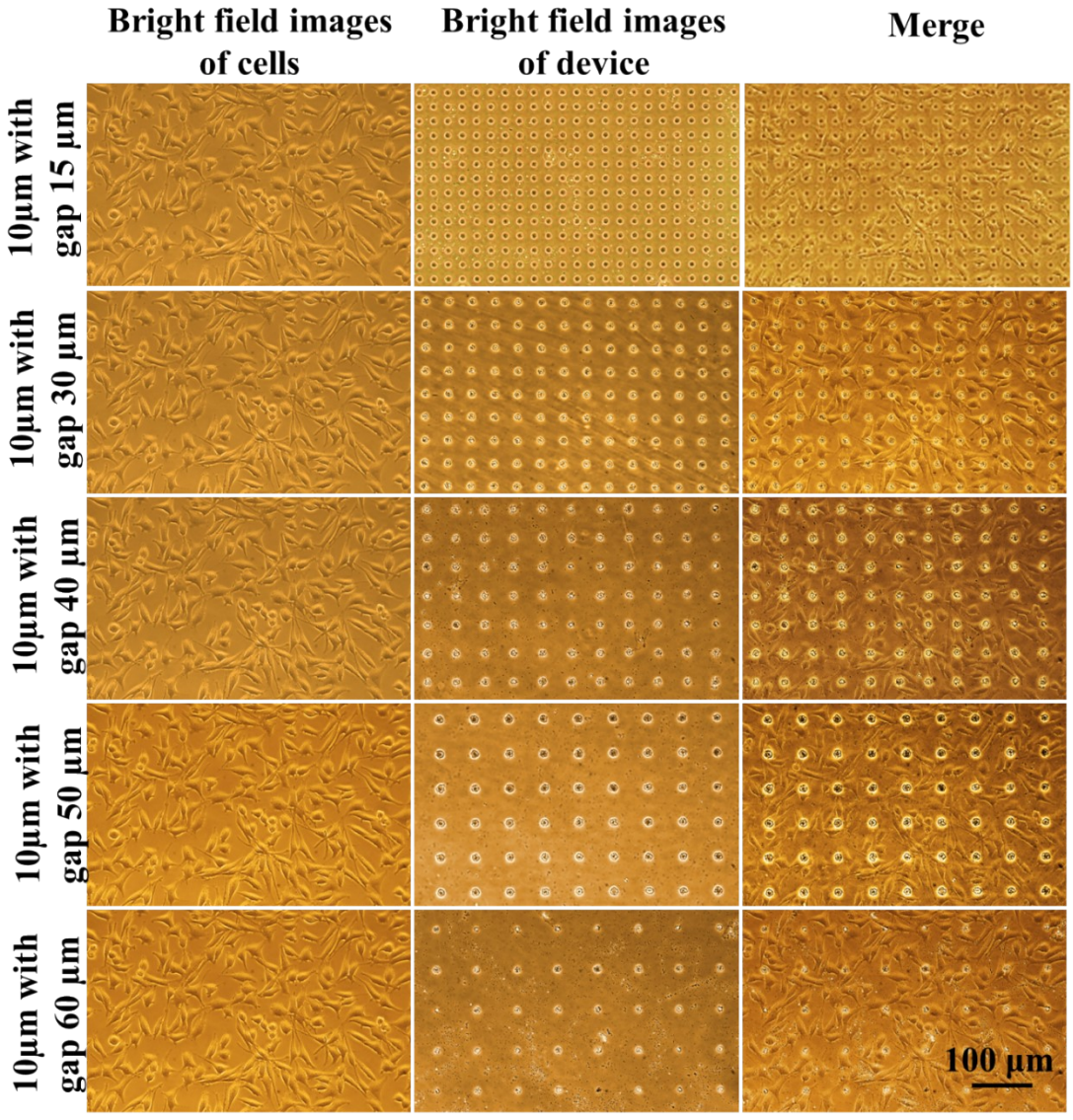

Figure S1. Bright field images of cells cultured on a cell culture plate merged with bright field images of the device for various inter-island spacings. It is noted that at an interisland spacing of 30 µm, almost all cells have a single contact point with the rGO island. On further increase of the inter-island spacing, there are some cells which doesn't have any contact point with the rGO island.

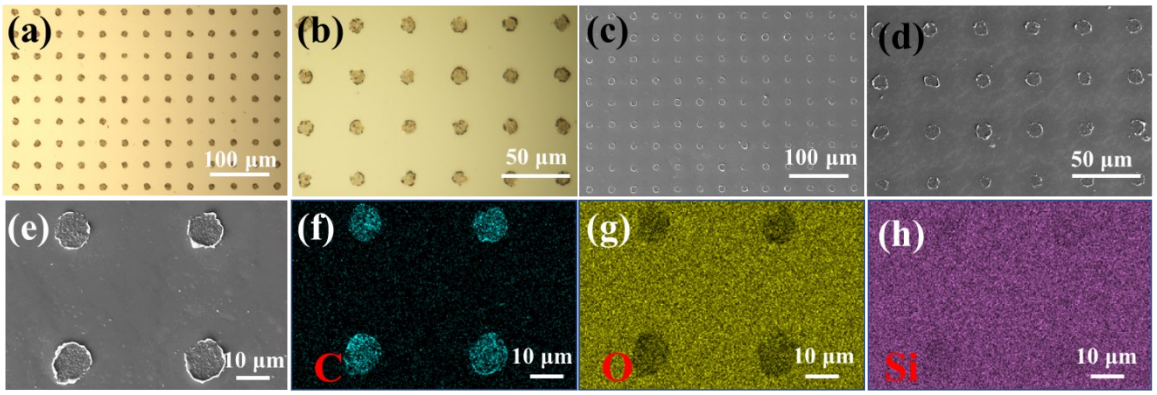

Figure S2. Images showing surface morphology and elemental integrity of the device after 5 reuse cycles. (a and b) Optical images with different magnification and corresponding SEM images (c and d). Images (f),(g), and (h) show the elemental EDS mapping for the elements Carbon (C), Oxygen (O), and Silicon (Si) corresponding to the SEM image (e).

To study the reusability and durability of the micropatterned rGO device, SEM analysis coupled with elemental mapping was performed after subjecting the device to 5 reuse cycles. As shown in optical images and SEM images **Figure S2**, the rGO device morphological features remained intact with minimal signs of degradation and delamination. Also, the elemental mapping confirms that the elemental compositions are maintained within the patterned area, indicating that patterned material(rGO) remains intact and immobilized with only minimal loss of patterned material by dispersion or leaching over repeated use. These results indicate that there is no structural or morphological damage that is happening to the device when the device is reused, also there is no change in elemental composition or the compositional fidelity. These results collectively indicate the cost-effectiveness, scalability, and resource efficiency of our platform for high-throughput photoporation-based intracellular delivery applications.

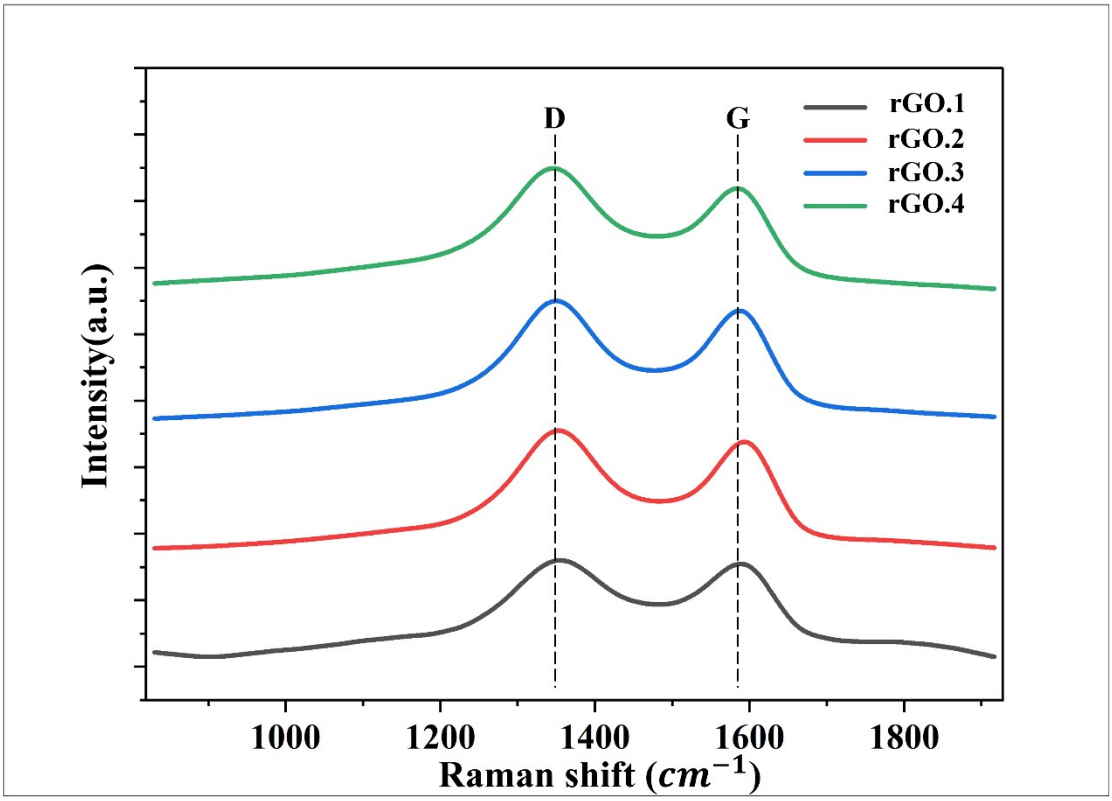

Figure S3. Confocal Raman spectra of reduced graphene oxide with different degree of reduction produced by varying the reduction duration. rGO.1, rGO.2. rGO.3 and rGO.4 corresponds to reduction duration of 60 min, 90 min, 120 min and 150 min respectively.

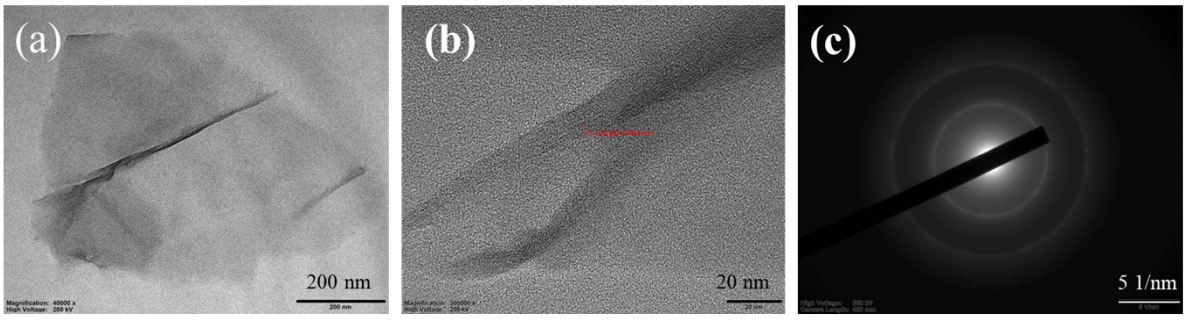

Figure S4. TEM characterization of UV-reduced graphene oxide. (a) Low-magnification TEM image showing thin, wrinkled rGO nanosheets. (b) High-resolution TEM image revealing disordered carbon lattice without long-range periodicity. (c) SAED pattern displaying diffuse concentric rings, confirming turbostratic stacking and limited crystallinity.

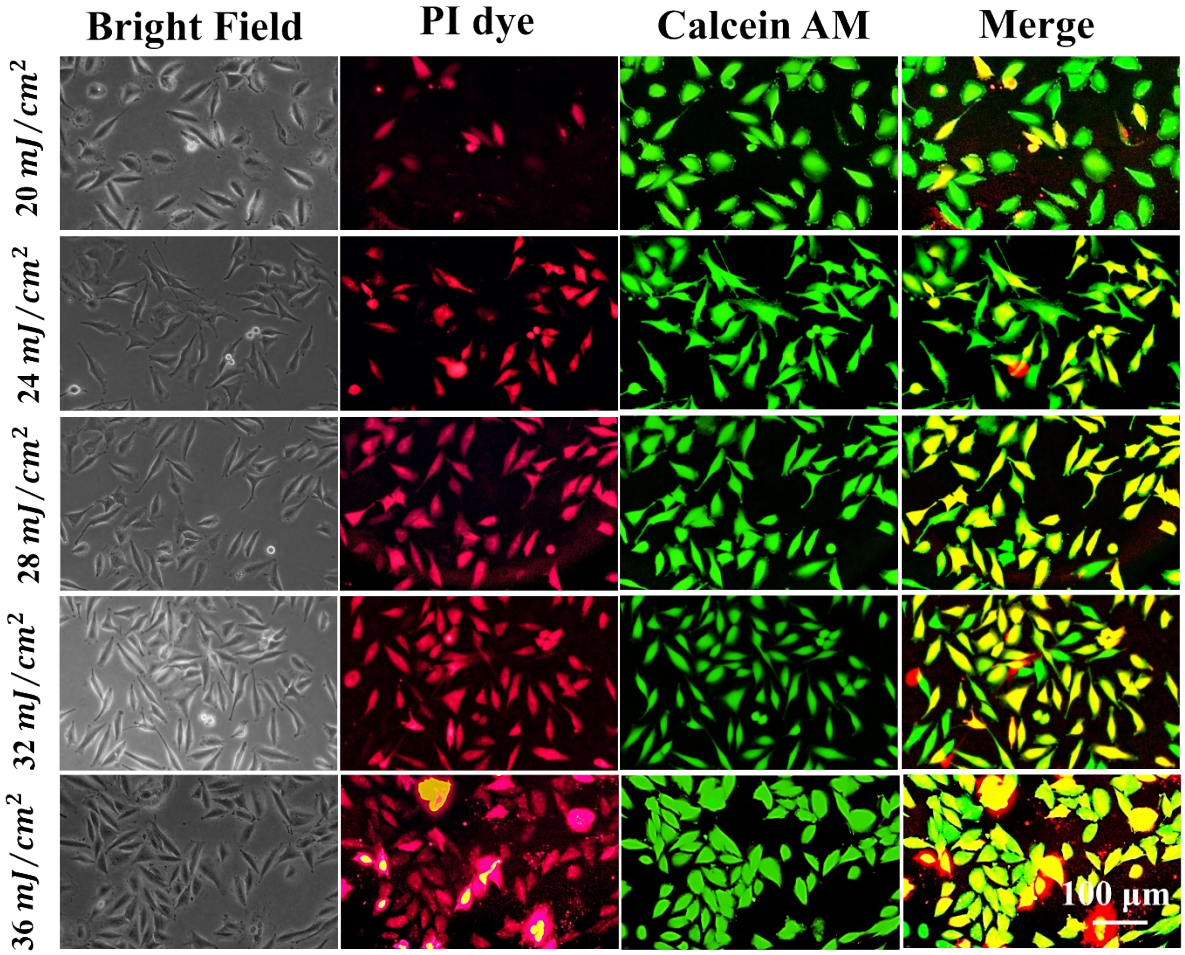

Figure S5. Optimisation of laser fluence. The figure shows intracellular delivery results for PI dye in LN-229 cells for varied laser fluence at a laser wavelength of 1064 nm, laser scanning speed of 15 mm/s. At a fluence of 28 mJ/cm^2, we achieve maximum delivery efficiency with minimal effects on cell viability, as the fluence further increases, cell viability decreases.

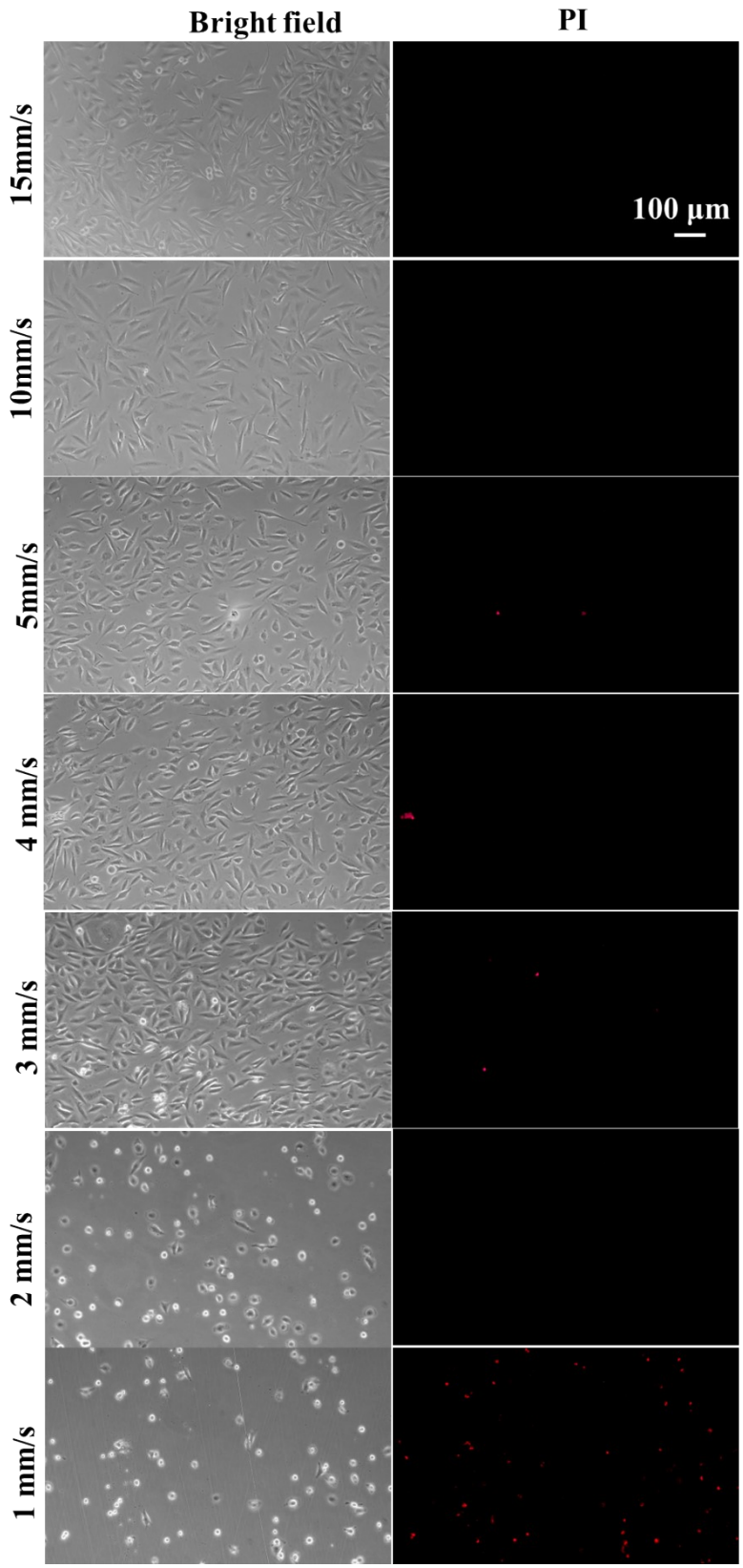

Figure S6. Optimization of laser scanning speed. The image shows brightfield and corresponding dead cell staining (PI dye) of the LN-229 cells, which underwent varied laser exposure at varied laser scanning speeds. Images were taken 30 minutes post-laser exposure. Results indicate there is no significant effect on cell viability until the scanning speed reduces to 3 mm/sec at optimised laser and device parameters.

Figure S6 shows the bright field images corresponding to the scanning speed optimization experiment performed in LN-229 cells. The cells were exposed to a laser with the rGO device, cells were stained with PI dye (dead cell staining) for 30 minutes post-exposure. We were able to see that a significant reduction of cell viability happens only when the laser scanning speed is reduced beyond 3 mm/s.

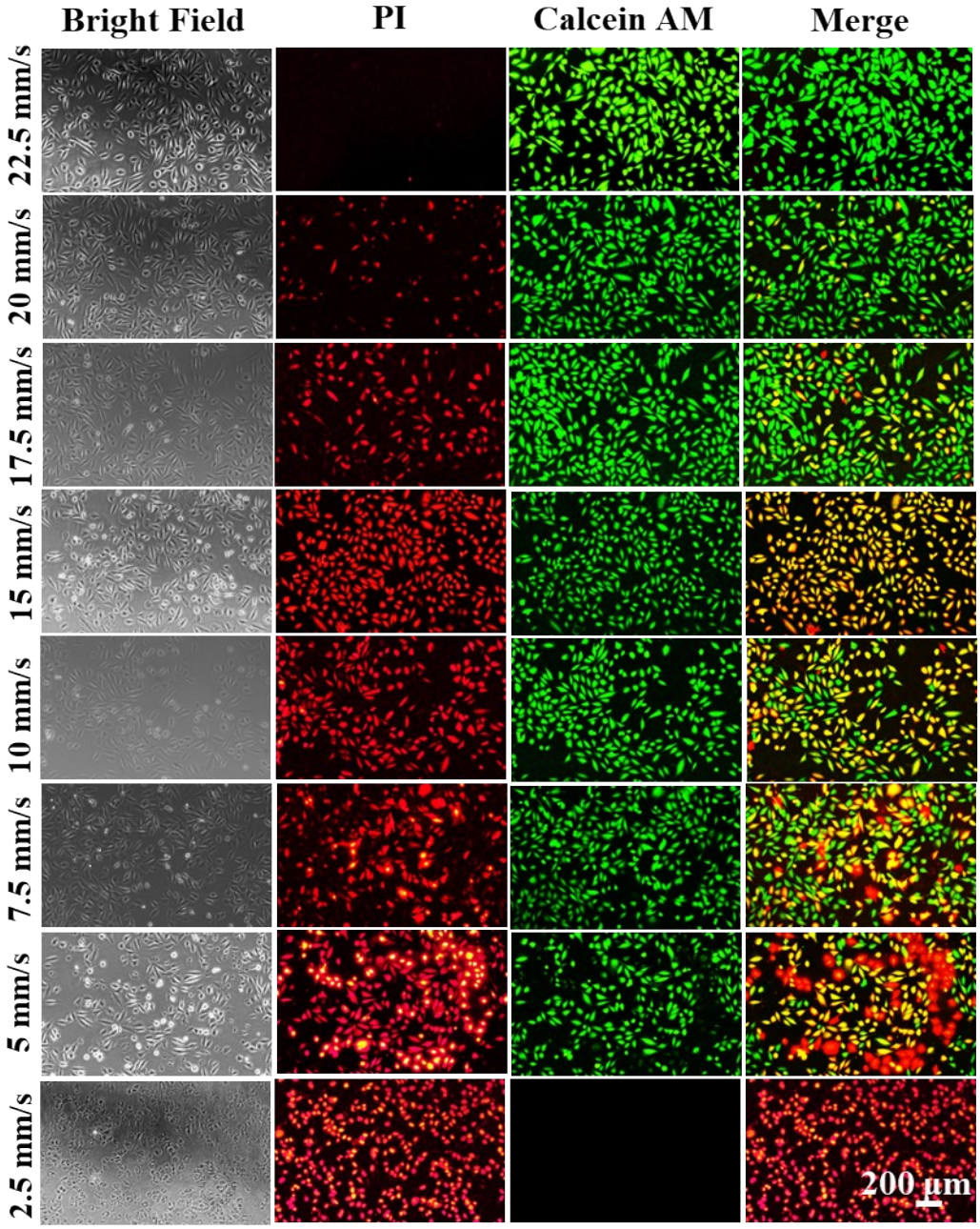

Figure S7. Optimization of laser scanning speed. Image shows brightfield and corresponding fluorescence images of the LN-229 cells which underwent PI delivery under varied laser scanning speed with fluence kept constant at 28 mJ/cm^2.

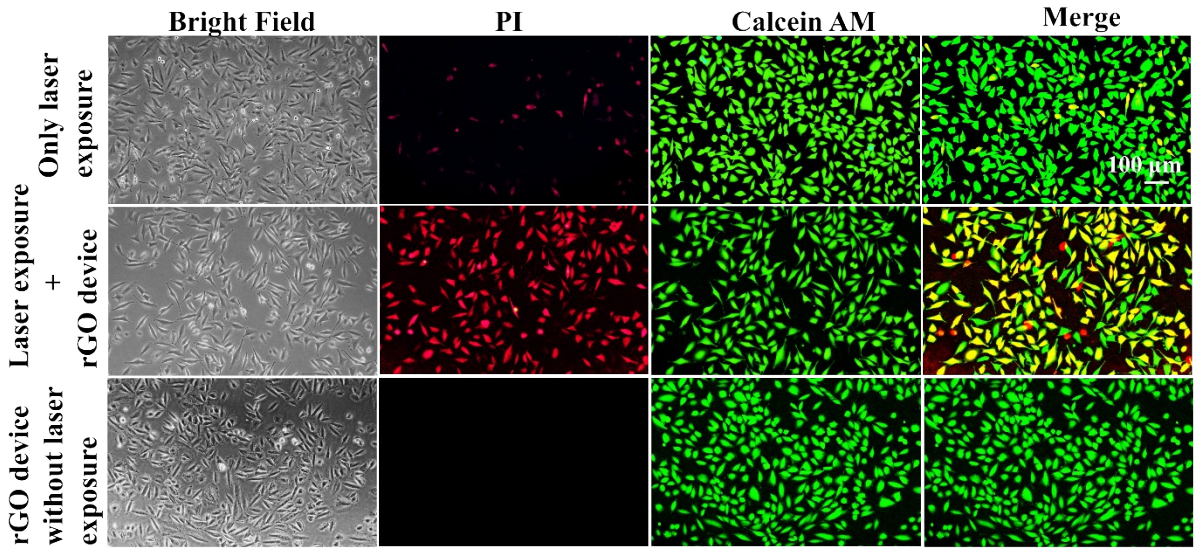

Figure S8. Control experiment showing the requirement of rGO device for intracellular delivery of PI at optimized laser parameters in LN229 cells. Bright field and fluorescence images of cells exposed to a laser with and without the rGO device, and cells exposed only to the rGO device. Red fluorescence in PI images shows the delivered cells, green fluorescence of cells in Calcein AM images shows viable cells, and in the merge image, yellow colour of cells shows delivered cells which are live, red colour indicates dead cells, and green colour indicates live and undelivered cells.

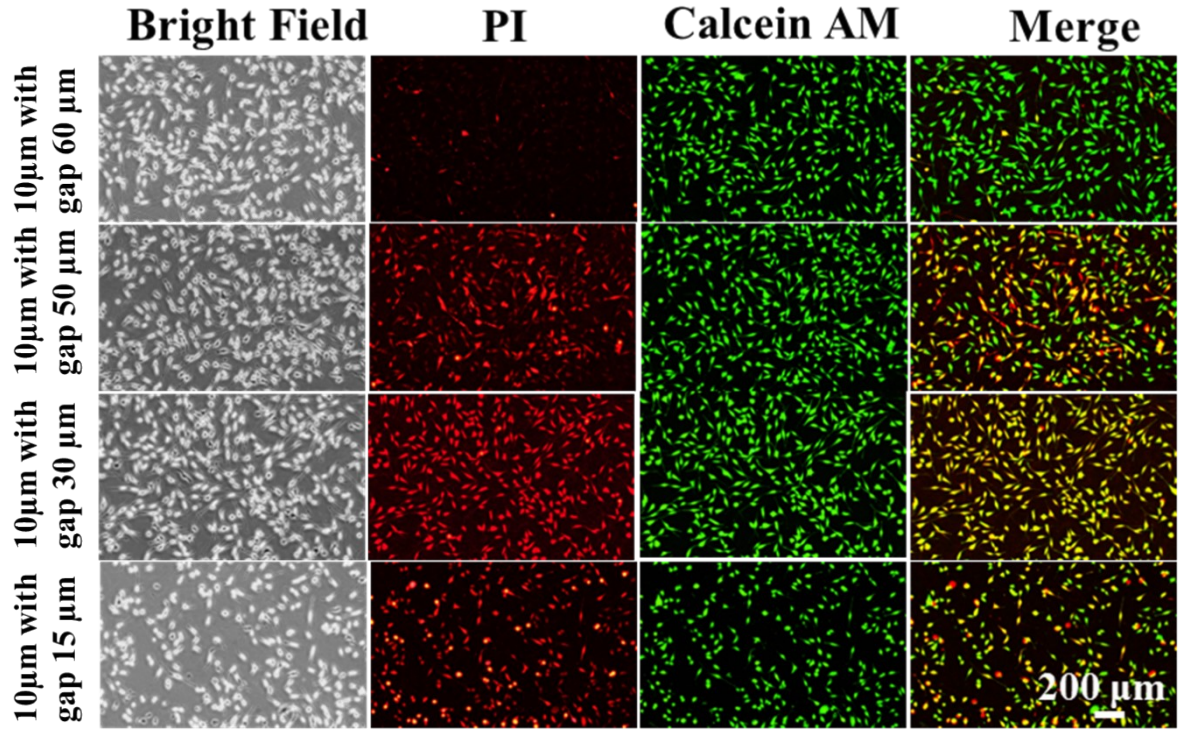

Figure S9. Bright field and fluorescent images corresponding to PI delivery experiments using rGO micropatterned devices with different interisland spacing performed in L929 cells. Images

indicate that higher than 30 µm inter-island spacing results in non-uniform delivery where whereas less than 30 µm inter-island spacing results in cell death.

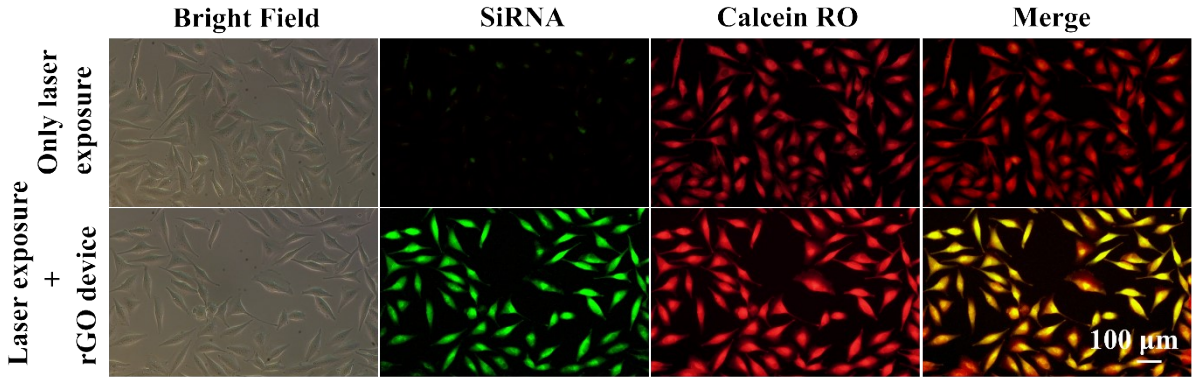

Figure S10. Control experiment showing the requirement of rGO device for intracellular delivery of siRNA at optimized laser parameters. Bright field and fluorescence images of LN-229 cells exposed to laser with and without rGO device. Green fluorescence in siRNA images shows the delivered cells, red-orange fluorescence of cells in Calcein red orange images shows viable cells and in merge image yellow to orangish yellow colour of cells shows delivered cells which are live, green colour indicates dead cells after delivery and red colour indicates live and undelivered cells.

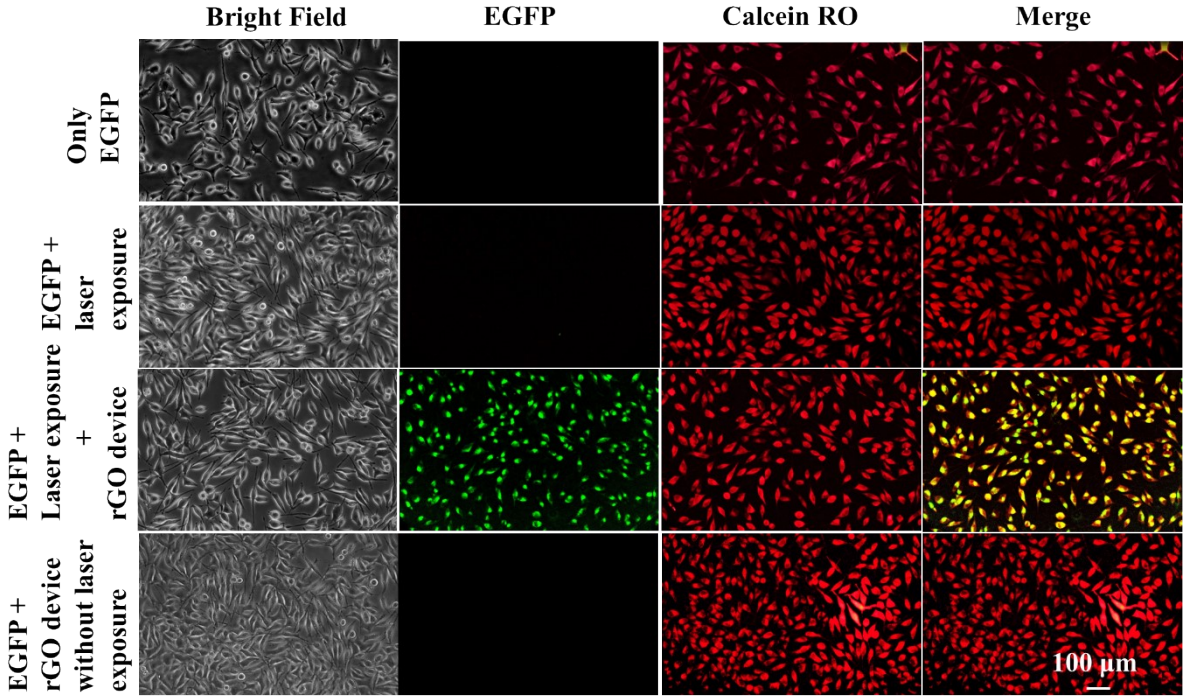

Figure S11. Control experiment showing the requirement of rGO device for intracellular delivery of plasmid for EGFP expression at optimized laser parameters(1064 nm,7 mm/s, and 28 mJ/cm^2). Bright field and fluorescence images of L929 cells incubated with EGFP but neither exposed to a laser nor to rGO device, L929 cells incubated with EGFP and exposed to a laser with and without rGO device, and images of L929 cells incubated with EGFP exposed to the rGO device but not to a laser. Green fluorescence in EGFP images indicates the delivered cells, while the red-orange fluorescence in Calcein red-orange images indicates viable cells. In the merged image, the yellow to orangish-yellow colour of cells indicates delivered cells that

are live. The green colour indicates dead cells after delivery, and the red colour indicates live and undelivered cells.

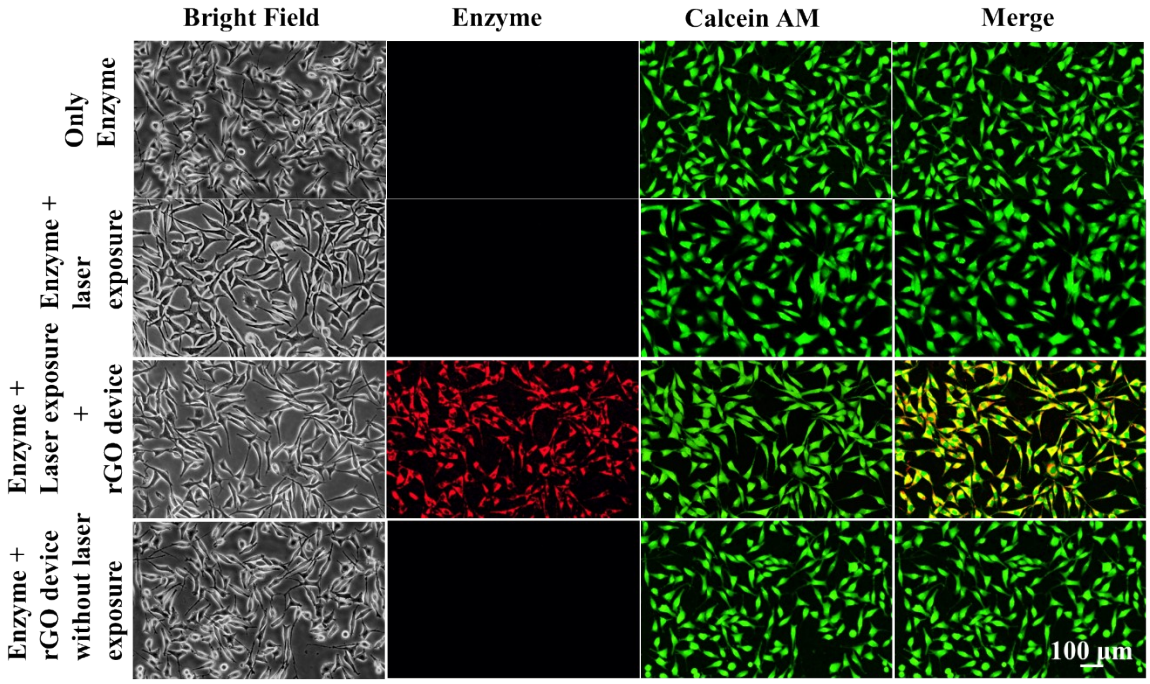

Figure S12. Control experiment showing the requirement of the rGO device for intracellular delivery of the enzyme at optimized laser parameters. Bright field and fluorescence images of L929 cells exposed to the laser with and without the rGO device. Green fluorescence in enzyme images shows the delivered cells, red-orange fluorescence of cells in Calcein red-orange images shows viable cells, and in the merge image, yellow to orangish yellow colour of cells shows delivered cells which are live, green colour indicates dead cells after delivery, and red colour indicates live and undelivered cells.

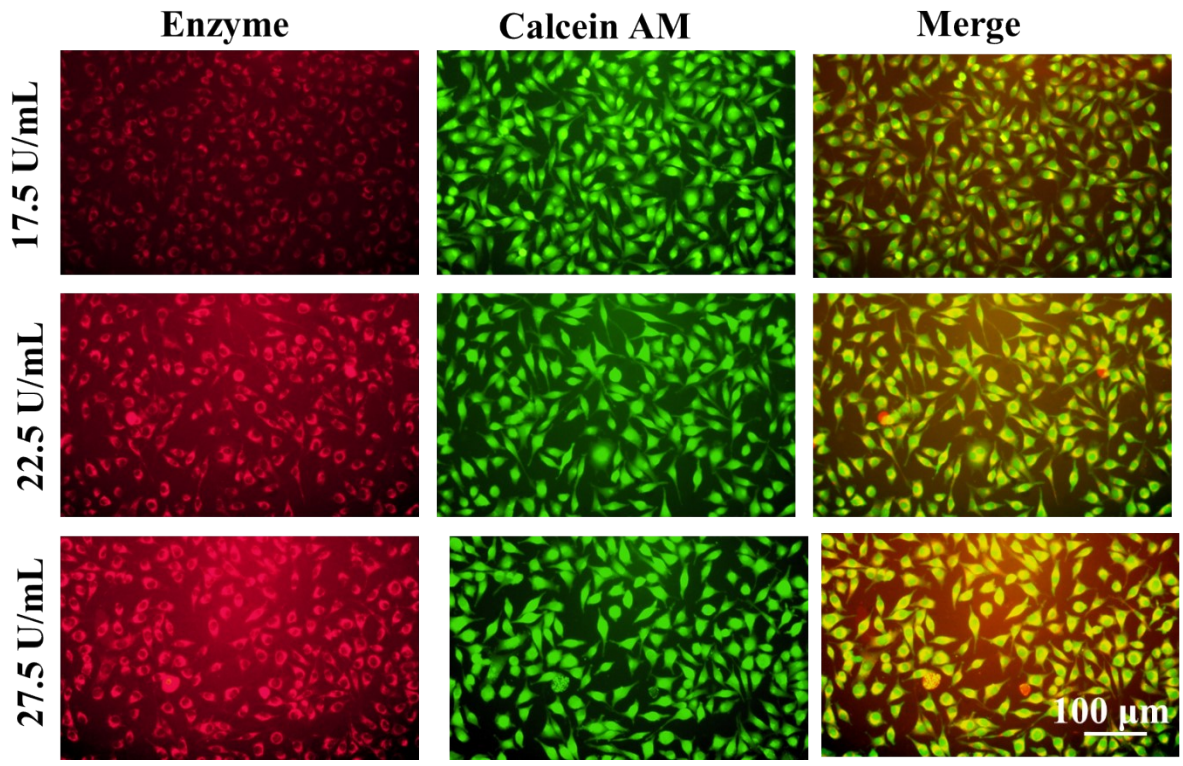

Figure S13: Fluorescent images corresponding to enzyme transfection for varied enzyme concentrations. Red fluorescence indicates enzyme transfected cells, green fluorescence indicates live cells and yellow- greenish yellow fluorescence in merged images indicate enzyme transfected live cells.

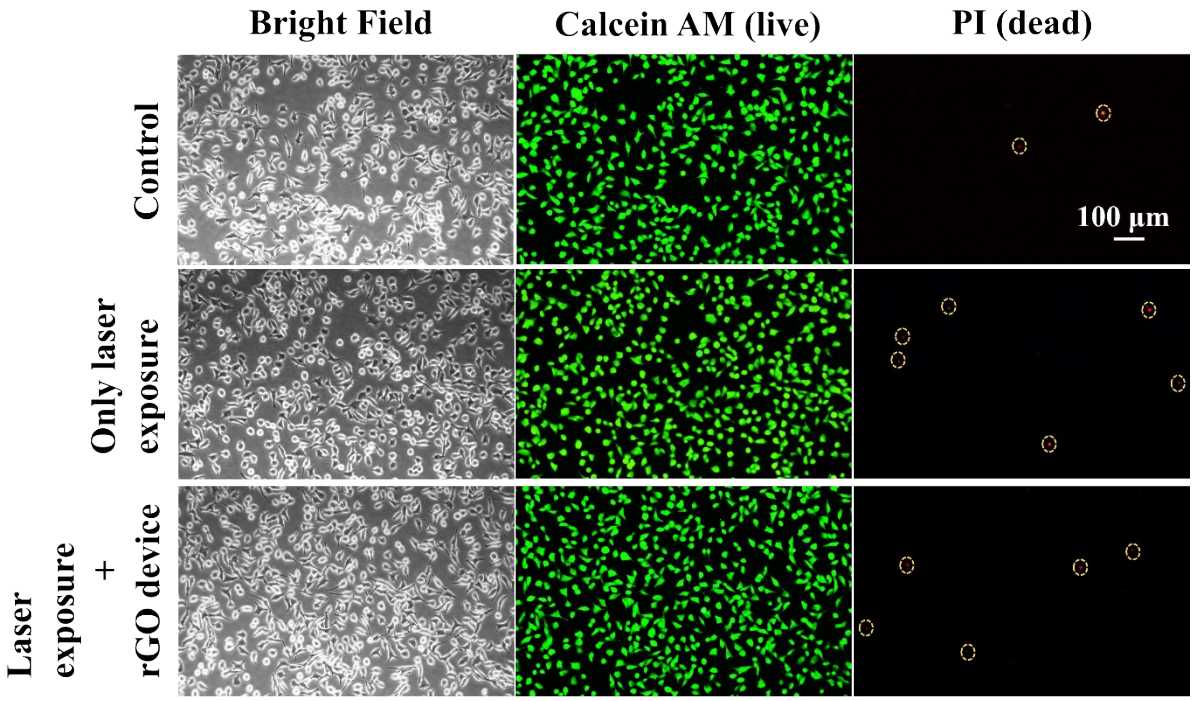

Figure S14. Biocompatibility studies for the rGO device-based optoporation platform(live-dead staining using calcein AM and PI dye). Bright field and fluorescent images of the cells which were neither subjected to laser exposure nor exposed to rGO device(first row, control), cells which were subjected to laser exposure without rGO device aligned on top of cells (second row) and cells which were subjected to laser exposure with rGO device (third row). (laser parameters-1064 nm, 28 mJ/cm^2 and 5 mm/s). Results indicate that our platform is biocompatible, as there are no significant effects on cell viability.

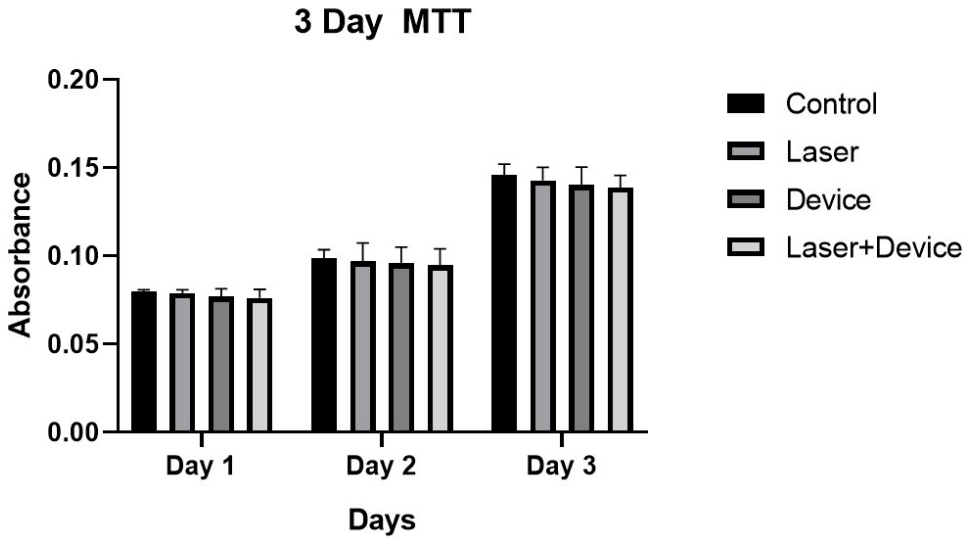

Figure S15: Quantification raw absorbance values of 3-day MTT assay for the SiHa cells that were neither subjected to laser exposure nor exposed to the rGO device (Control), cells that were subjected to laser exposure without the micro-patterned rGO device (Laser), cells exposed to rGO device with no laser exposure (Device), and cells that were subjected to laser exposure with the micro-patterned rGO device aligned on top of cells (Device+Laser). Data represent mean ± SD (n = 3). MTT assay results (mean ± SD, n = 3) show a progressive increase in (absorbance) metabolic activity from Day 1 to Day 3 across all groups

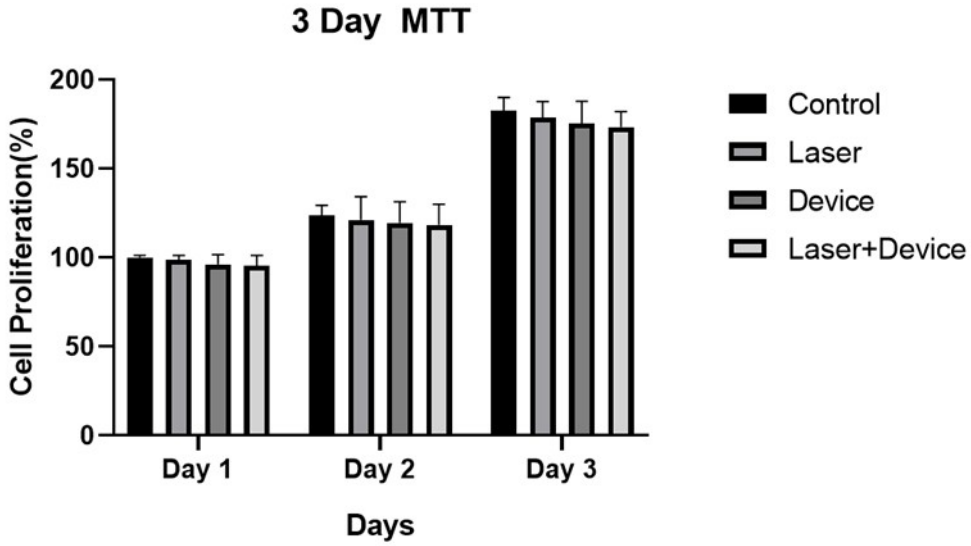

Figure S16: Quantification cell proliferation from 3-day MTT assay for the SiHa cells that were neither subjected to laser exposure nor exposed to the rGO device (Control), cells that were subjected to laser exposure without the micro-patterned rGO device (Laser), cells exposed to rGO device with no laser exposure (Device), and cells that were subjected to laser exposure with the micro-patterned rGO device aligned on top of cells (Device+Laser). Data represent mean ± SD (n = 3). MTT assay results (mean ± SD, n = 3) show a progressive increase in metabolic activity from Day 1 to Day 3 across all groups.

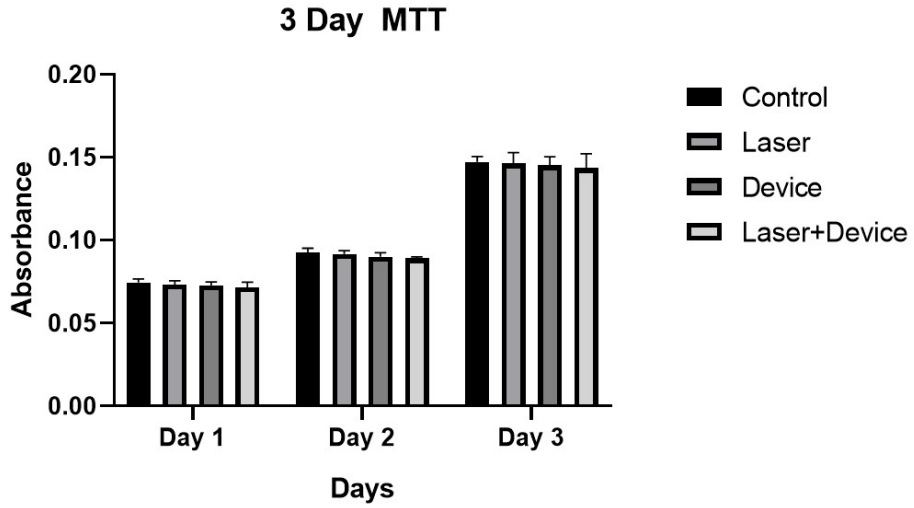

Figure S17: Quantification of raw absorbance values of 3-day MTT assay for the LN229 cells that were neither subjected to laser exposure nor exposed to the rGO device (Control), cells that were subjected to laser exposure without the micro-patterned rGO device (Laser), cells exposed to the rGO device with no laser exposure (Device), and cells that were subjected to laser exposure with the micro-patterned rGO device aligned on top of cells (Device+Laser). Data represent mean ± SD (n = 3). MTT assay results (mean ± SD, n = 3) show a progressive increase in (absorbance) metabolic activity from Day 1 to Day 3 across all groups

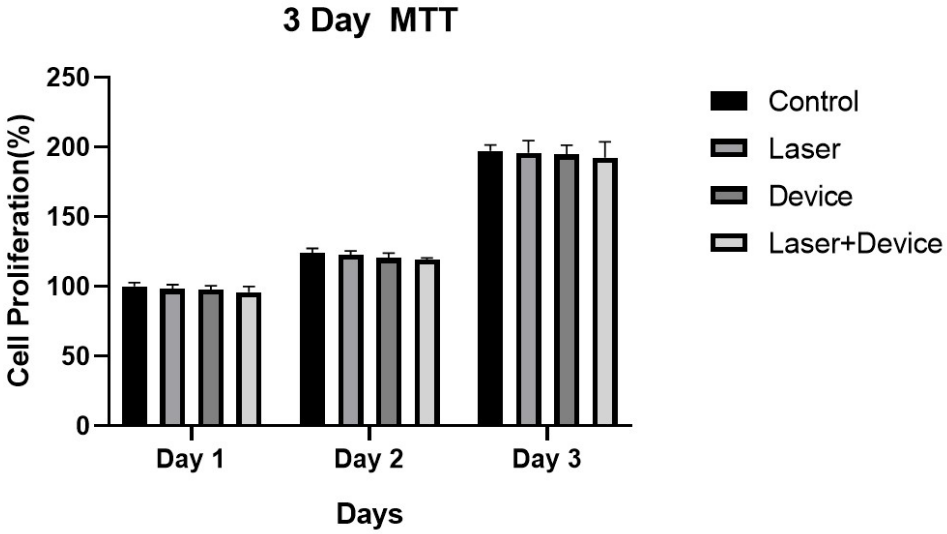

Figure S18: Quantification cell proliferation from 3-day MTT assay for the LN229 cells that were neither subjected to laser exposure nor exposed to the rGO device (Control), cells that were subjected to laser exposure without the micro-patterned rGO device (Laser), cells exposed to the rGO device with no laser exposure (Device), and cells that were subjected to laser exposure with the micro-patterned rGO device aligned on top of cells (Device+Laser). Data represent mean ± SD (n = 3). MTT assay results (mean ± SD, n = 3) show a progressive increase in metabolic activity from Day 1 to Day 3 across all groups

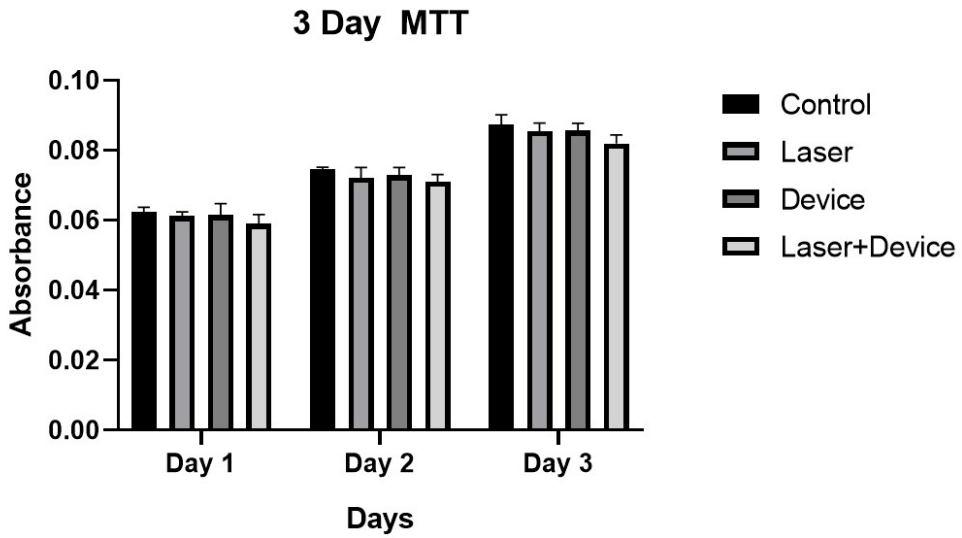

Figure S19: Quantification of raw absorbance values of 3-day MTT assay for the L929 cells that were neither subjected to laser exposure nor exposed to the rGO device (Control), cells that were subjected to laser exposure without the micro-patterned rGO device (Laser), cells exposed to the rGO device with no laser exposure (Device), and cells that were subjected to laser exposure with the micro-patterned rGO device aligned on top of cells (Device+Laser). Data represent mean ± SD (n = 3). MTT assay results (mean ± SD, n = 3) show a progressive increase in (absorbance) metabolic activity from Day 1 to Day 3 across all groups

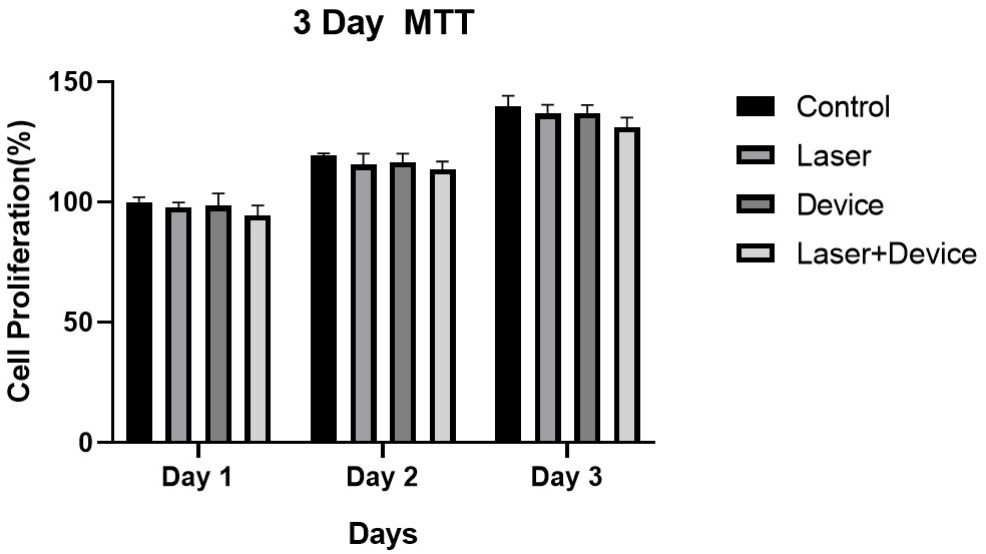

figure S20: Quantification cell proliferation from 3-day MTT assay for the L929 cells that were neither subjected to laser exposure nor exposed to the rGO device (Control), cells that were subjected to laser exposure without the micro-patterned rGO device (Laser), cells exposed to rGO device with no laser exposure (Device), and cells that were subjected to laser exposure with the micro-patterned rGO device aligned on top of cells (Device+Laser). Data represent mean ± SD (n = 3). MTT assay results (mean ± SD, n = 3) show a progressive increase in metabolic activity from Day 1 to Day 3 across all groups

Table Analyzed	3 Day MTT				
Two-way RM ANOVA	Matching: Stacked				
Assume sphericity?	No				
Alpha	0.05				
Source of Variation	% of total variation	P value	P value summary	Significant?	Geisser-Greenhouse's epsilon
Interaction	0.1637	0.9696	ns	No	
Day	94.32	<0.0001	****	Yes	0.7204
Sample	2.145	0.0381	*	Yes	
Subject	1.252	0.3661	ns	No	
ANOVA table	SS	DF	MS	F (DFn, DFd)	P value
Interaction	603.9	6	100.7	F (6, 16) = 0.2065	P=0.9696
Day	347917	2	173958	F (1.441, 11.53) = 356.9	P<0.0001
Sample	7912	3	2637	F (3, 8) = 4.567	P=0.0381
Subject	4620	8	577.5	F (8, 16) = 1.185	P=0.3661
Residual	7798	16	487.4		
Data summary					
Number of columns (Sample)	4				
Number of rows (Day)	3				
Number of subjects (Subject)	12				

Table S1. Two-way RM ANOVA results

Table S2. Tukey's multiple comparisons test.

Tukey's multiple comparisons test	Mean Diff.	95.00% CI of diff.	Significant?	Summary	Adjusted P Value
Day 1					
Control vs. Laser	13.00	-29.40 to 55.40	No	ns	0.6336
Control vs. Device	9.333	-98.61 to 117.3	No	ns	0.9622
Control vs. Laser+Device	34.33	-48.98 to 117.6	No	ns	0.3494
Laser vs. Device	-3.667	-112.6 to 105.3	No	ns	0.9973
Laser vs. Laser+Device	21.33	-62.69 to 105.4	No	ns	0.6366
Device vs. Laser+Device	25.00	-75.47 to 125.5	No	ns	0.7417
Day 2					
Control vs. Laser	23.67	-83.63 to 131.0	No	ns	0.5961
Control vs. Device	17.33	-62.53 to 97.19	No	ns	0.6307
Control vs. Laser+Device	35.67	-38.51 to 109.8	No	ns	0.2184
Laser vs. Device	-6.333	-94.38 to 81.71	No	ns	0.9889
Laser vs. Laser+Device	12.00	-75.50 to 99.50	No	ns	0.9310
Device vs. Laser+Device	18.33	-53.35 to 90.02	No	ns	0.7372
Day 3					
Control vs. Laser	18.67	-68.53 to 105.9	No	ns	0.8121
Control vs. Device	17.00	-68.84 to 102.8	No	ns	0.8321
Control vs. Laser+Device	54.00	-34.63 to 142.6	No	ns	0.2003
Laser vs. Device	-1.667	-74.64 to 71.30	No	ns	0.9997
Laser vs. Laser+Device	35.33	-43.95 to 114.6	No	ns	0.3835
Device vs. Laser+Device	37.00	-39.41 to 113.4	No	ns	0.3243

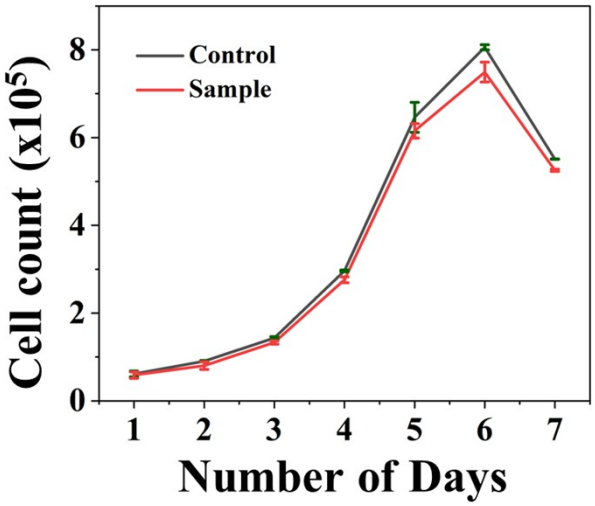

Figure S21. Cell proliferation profile after photoporation, assessed using flow cytometry. Data are shown as mean ± SD (n = 3).

To assess the long-term effects of our photoporation platform using the rGO micropatterned device, cell proliferation was studied for 7 days post-photoporation, starting from the time point immediately after the photoporation. As shown in Figure S21 cell count gradually increased for the sample treated with photoporation, indicating the sustained viability and active proliferation of the cells after transient cell membrane permeabilization by the rGO micropatterned device-mediated photoporation. The cell proliferation profile shows a steep decrease in the cell count after the 6th day and it was attributed to the confluency-induced growth arrest. When compared with an untreated control, there is only a slight reduction in cell count, which indicates that our platform is biocompatible and allows the proliferation ability of the cells to remain unaffected. The use of flow cytometry helped in the accurate and precise quantification of cell proliferation.